

Nonlinear Hall Effects in Strained Twisted Bilayer WSe₂

Jin-Xin Hu¹, Cheng-Ping Zhang¹, Ying-Ming Xie¹, and K. T. Law^{1*}

Department of Physics, Hong Kong University of Science and Technology, Clear Water Bay, Hong Kong, China

(Dated: December 22, 2024)

Recently, it has been pointed out that the twisting of bilayer WSe₂ would generate topologically non-trivial flat bands near the Fermi energy. In this work, we show that twisted bilayer WSe₂ (tWSe₂) with uniaxial strain exhibits a large nonlinear Hall (NLH) response due to the non-trivial Berry curvatures of the flat bands. Moreover, the NLH effect is greatly enhanced near the topological phase transition point which can be tuned by a vertical displacement field. Importantly, the nonlinear Hall signal changes sign across the topological phase transition point and provides a way to identify the topological phase transition and probe the topological properties of the flat bands. The strong enhancement and high tunability of the NLH effect near the topological phase transition point renders tWSe₂ and related moire materials new platforms for rectification and second harmonic generations.

Introduction

The study of long-period moiré superlattices formed in van der Waals heterostructures has emerged as a central topic in condensed matter physics[1]. After the observation of correlated insulator and superconductivity in twisted bilayer graphene(TBG) with flat bands[2–13], it was proposed that there are moiré-mediated flat bands in twisted transition metal dichalcogenide heterobilayers and homobilayers[14, 15]. Recently, correlated insulating phases and superconductivity were discovered in twisted bilayer tungsten diselenide (tWSe₂) at twist angles between 4° to 5°[16, 17].

Besides the correlated phases, it was shown that the flat bands of the moire superlattices also exhibit non-trivial topological properties. For example, at 3/4 filling in hBN-aligned TBG, the degeneracy of the bands with non-trivial Chern numbers is lifted by electron-electron interactions and results in quantum anomalous Hall states which were observed recently [18–20]. These observations clearly demonstrate that the topological properties of the flat bands also have important consequences on the nature of the correlated phases.

Similar to TBG, it was pointed out that flat bands with non-trivial Chern numbers can be generated in tWSe₂ and a couple of topological insulating phases were predicted at a wide range of twist angles[15]. As in the case of TBG, the topology of the bands would affect the nature of the insulating phase when the bands are half filled and the interaction effects are strong. In this work, we propose that the nonlinear response in electric field can be used to unveil the topological properties of the flat bands and identify the topological phase transition point through the measurements of the nonlinear Hall (NLH) effect.

The NLH effect is a fascinating phenomenon recently proposed by Sodemann and Fu[21], and experimentally observed in bilayer and multilayer WTe₂[22, 23]. It is the generation of a transverse DC current and a transverse voltage with frequency 2ω when an AC current of

frequency ω is applied, which has potential applications in rectifications and second harmonic generations. The effect originates from the non-vanishing dipole moment of the Berry curvature of the bands which characterizes the second-order nonlinear hall susceptibility. In pristine tWSe₂, regardless of how large the Berry curvatures of the bands are, the three fold rotational symmetry forces the Berry curvature dipole to be zero and the NLH effect vanishes. However, we demonstrate here that a small strain breaks the three-fold rotational symmetry and generates a large Berry curvature dipole. Importantly, these symmetry breaking strain effects have been observed recently in experiments[24]. Moreover, the Berry curvature dipole is strongly enhanced and has opposite signs across the topological phase transition point when the top two valence bands touch each other and exchange Berry curvatures[25]. As the topological phase transition can be tuned by a vertical displacement field, the measurement of the NLH effect can serve as a probe of the topological phase transition in tWTe₂. Moreover, the strong enhancement and the highly tunability of the NLH effect by a displacement field renders tWSe₂ and related moire materials new platforms for rectification and second harmonic generations applications.

The rest of our paper is organized as follows. First, we present the continuum model of tWSe₂ which takes into account a uniaxial strain in the bottom layer induced by substrate or external modulation, which breaks the three-fold rotational symmetry such that nonzero Berry curvature dipole can be created. Second, we calculate the Berry curvature dipole in the presence of strain. We show that the strained tWSe₂ exhibits large nonlinear Hall response. Third, we explore the behavior of the NLH response near the topological phase transition induced by a displacement field. We find that the Berry curvature dipole is strongly enhanced near the topological phase transition point and it changes sign across the transition point.

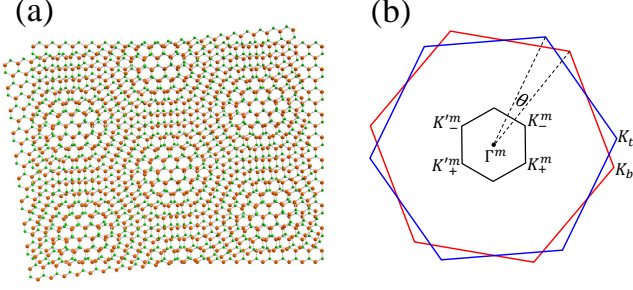


FIG. 1: (a) A schematic figure of tWSe₂ moiré superlattice at a twist angle of 7°. (b) The original Brillouin zone of bottom (red) and top (blue) layers and the folded moiré Brillouin zone (black).

Continuum model of strained tWSe₂

We consider a AA stacking bilayer WSe₂ with lattice constant a_0 in a single layer and at a twist angle θ . A schematic figure is shown in Fig. 1a. The moiré superlattice, which has a moiré lattice constant $L_M = a_0/2\sin\frac{\theta}{2}$, folds the energy bands and gives rise to the so-called moiré Brillouin zone (see Fig. 1b). These moiré energy bands originating from the K_+ or K_- valleys can be described by the continuum Hamiltonian[15] $H = \sum_{\xi} \int d\mathbf{r} \psi_{\xi}^{\dagger}(\mathbf{r}) \hat{\mathcal{H}}_{\xi}(\mathbf{r}) \psi_{\xi}(\mathbf{r})$ with

$$\hat{\mathcal{H}}_{\xi}(\mathbf{r}) = \begin{pmatrix} \hat{H}_{b,\xi} + \Delta_b(\mathbf{r}) & T_{\xi}(\mathbf{r}) \\ T_{\xi}^{\dagger}(\mathbf{r}) & \hat{H}_{t,\xi} + \Delta_t(\mathbf{r}) \end{pmatrix}. \quad (1)$$

Here, $\xi = \pm$ is the valley index denoting whether the bands originate from the K_+ or K_- valleys of the monolayer Brillouin zone. The electron creation operators are denoted as $\psi_{\xi}^{\dagger} = (\psi_{b,\xi}^{\dagger}, \psi_{t,\xi}^{\dagger})$, where t and b label the top and bottom layers respectively. It is important to note that due to the large Ising spin-orbit coupling in 2H-structure WSe₂, the top valence band of monolayer WSe₂ K_+ and K_- valleys are fully spin polarized and have opposite spin. Therefore, the spin and valley indices are locked together and the spin-index is dropped. As a result, the Hamiltonian of a single layer at valley ξ can be written as

$$\hat{H}_{l,\xi} = -\frac{\hbar^2}{2m^*}(\hat{\mathbf{k}} - \mathbf{K}_{\xi,l}^m)^2 - l\frac{V_z}{2}, \quad (2)$$

where $l = +1(-1)$ labels the bottom(top) layer, m^* is the effective mass of valence band, and V_z is the staggered layer potential generated by the vertical displacement field. The intra-layer moiré potential and the coupling between the two layers are denoted as $\Delta_l(\mathbf{r})$ and $T_{\xi}(\mathbf{r})$ respectively which can be written as:

$$\Delta_l(\mathbf{r}) = V \sum_{i=1,2,3} e^{i(\mathbf{g}_i \cdot \mathbf{r} + l\psi)} + h.c., \quad (3)$$

$$T_{\xi}(\mathbf{r}) = w(1 + e^{-i\xi\mathbf{g}_2 \cdot \mathbf{r}} + e^{-i\xi(\mathbf{g}_1 + \mathbf{g}_2) \cdot \mathbf{r}}). \quad (4)$$

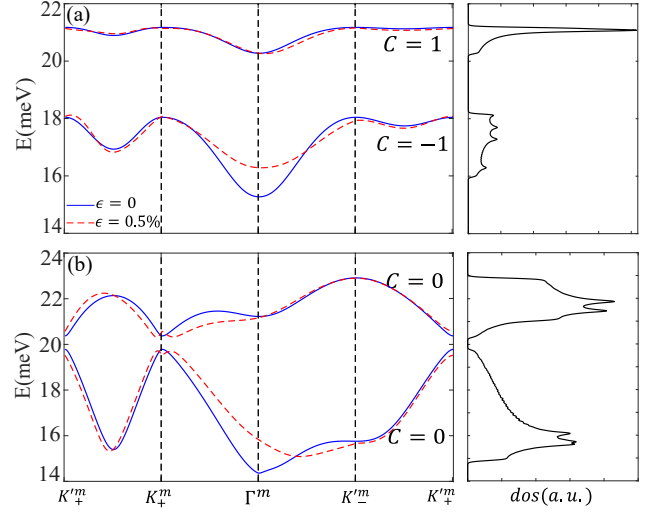


FIG. 2: (a) The band structure of tWSe₂ at $\theta = 1.4^\circ$ with (dashed red lines) and without (solid blue lines) strain. The staggered potential $V_z = 0$ and the top two valence bands originating from K_+ valleys of the original monolayer Brillouin zone have opposite Chern numbers. The bands originating from the K_- valleys are related to the K_+ valley bands by time-reversal which are not shown above. (b) The band structure with $V_z = 5$ meV with (dashed red lines) strain and without (solid blue lines) strain. As V_z increases, a topological phase transition happens at $V_z \approx 4.2$ meV and the two top valence bands exchange Chern numbers and results in topologically trivial flat bands.

Here, V and ψ , characterize the amplitude and phase of the moiré potentials respectively, w characterizes the tunneling strength between the top and bottom layers, and the moiré reciprocal lattice vectors are $\mathbf{g}_i = \frac{4\pi}{\sqrt{3}L_M}(\cos\frac{2(i-1)\pi}{3}, \sin\frac{2(i-1)\pi}{3})$. We adopt the model parameters from ref. [15] (a_0, m^*, w, V, ψ) = (3.32 Å, 0.44 m_e , 9.7 meV, 8.9 meV, 91°), which are estimated from the first principle calculations.

It is important to note that the Berry curvature dipole transforms as a pseudo-vector which vanishes in the presence of a three-fold rotational symmetry as discussed in detail in the next section. In realistic systems, the three-fold symmetry in tWSe₂ can be broken by the substrate induced or externally applied strain. The strain induced symmetry breaking has been observed experimentally[24]. Therefore, we introduce a strain field on the bottom layer to describe the strain effect. Specifically, the strain tensor $\boldsymbol{\mathcal{E}}$ is a two-dimensional matrix, which can be written as[26]:

$$\boldsymbol{\mathcal{E}} = \epsilon \begin{pmatrix} \cos^2 \varphi - \nu \sin^2 \varphi & (1 + \nu) \cos \varphi \sin \varphi \\ (1 + \nu) \cos \varphi \sin \varphi & \sin^2 \varphi - \nu \cos^2 \varphi \end{pmatrix}. \quad (5)$$

The angle φ denotes the in-plane direction of the uniaxial strain direction with respect to the zigzag edge of the sample and ϵ characterizing the strength of strain, and

$\nu = 0.19$ is the poisson ratio for WSe₂[27].

The strain has two important effects shifting the Dirac point for bottom layer WSe₂ to $\mathbf{D}_\xi = (I - \boldsymbol{\epsilon}^T)\mathbf{K}_\xi - \xi\mathbf{A}$ and generating an effective gauge field $\mathbf{A} = \frac{\sqrt{3}}{2a_0}\beta(\epsilon_{xx} - \epsilon_{yy}, -2\epsilon_{xy})$. Here, β is taken as 2.30 in our calculations according to previous first principle calculations for strained monolayer WSe₂ [26, 28]. As a result, the continuum Hamiltonian of this strained tWSe₂ is obtained by replacing \hat{H}_b in Eq. 1 as

$$\hat{H}_{b,\xi} = -\frac{\hbar^2}{2m^*}((I + \boldsymbol{\epsilon}^T)(\hat{\mathbf{k}} - \mathbf{D}_\xi^m))^2 - \frac{V_z}{2}. \quad (6)$$

To estimate the range of strain ϵ within which our model is valid, we expect that the strain induced shifting of the Dirac point would be smaller than the separation of the Dirac points due to twisting. With a twist angle θ , the separation of the Dirac point K in momentum space is $\Delta K = |K|\theta$, and the shift of the K point by uniaxial strain is $\Delta K_s \approx \epsilon|K|$. Therefore, the strain effect can be treated as a perturbation to the moiré super-lattice when $\epsilon \ll \theta$. In our calculations below, we assume that the strain induces a 0.5% change in the lattice constant of the bottom layer WSe₂ along the direction of the strain such that $\epsilon \approx 0.2\theta$.

In Fig. 2a, we show the moiré energy bands of tWSe₂ with twist angle $\theta = 1.4^\circ$ with and without strain. The top two valence bands originating from the K_+ valley of the monolayer Brillouin zones carry finite Chern numbers $C = 1$ and $C = -1$ respectively when $V_z = 0$. Due to time-reversal symmetry, the top two valence bands originating from the K_- valleys carry Chern numbers $C = -1$ and $C = 1$ respectively. As the two valleys do not couple in momentum space, one can define a Z_2 topological invariant as $Z_2 = |(C_{K_+} - C_{K_-})/2|$ to describe the topological properties of the bulk bands, where C_K is the Chern number of the top valence band originating from the K valleys of the monolayer Brillouin zone. In Fig. 2b, a staggered potential of $V_z = 5$ meV induces a topological phase transition and the system becomes topologically trivial. The band structure with and without strain are depicted. It is important to note that the strain with $\epsilon = 0.5\%$ is not sufficient to close the band gap and the topological properties of the flat bands are not changed by strain. Moreover, the energy dependence of the density of states for $V_z = 0, 5$ meV are also shown on the right side of Fig. 2, which is important to determine the occupation number of holes n_h as discussed below.

Nonlinear Hall response

In this section, we consider the NLH response for tWSe₂. The NLH effect is characterized by the generation of a transverse voltage using a charge current in time-reversal invariant systems without external magnetic fields or magnetic orders. Moreover, this effect is

nonlinear in nature and exhibits a quadratic current-voltage relation. More specifically, when an electric field $\mathbf{E}(t) = \frac{1}{2}(\epsilon e^{i\omega t} + \epsilon^* e^{-i\omega t})$ with the amplitude vector ϵ and frequency ω is applied, the Hall current has both rectified and second-harmonic components $J_{y(x)}^{(0)} = \chi_{yxx(xy)}\epsilon_{x(y)}\epsilon_{x(y)}^*$ and $J_{y(x)}^{(2)} = \chi_{yxx(xy)}\epsilon_{x(y)}\epsilon_{x(y)}$, where χ is the nonlinear Hall susceptibility. As shown in ref. [21, 29, 30], the nonlinear Hall susceptibility can be written as:

$$\chi_{yxx(xy)} = \mp \frac{e^3 \tau}{2(1 + i\omega\tau)} D_{x(y)} \quad (7)$$

where τ is the relaxation time. The Berry curvature dipole D_i are elements of the Berry curvature dipole pseudo-vector. In strictly two dimensions, it is given by

$$D_i = - \int \frac{d\mathbf{k}}{(2\pi)^2} \sum_{n,\xi=\pm 1} v_{n\mathbf{k},\xi}^i \Omega_{n\mathbf{k},\xi} \frac{\partial f(E_{n\mathbf{k},\xi})}{\partial E}, \quad (8)$$

where n as the band index and v^i as the Fermi velocity of the Bloch state, and the Berry curvature can be obtained from Bloch wavefunctions as:

$$\Omega_{n\mathbf{k},\xi} = i \langle \partial_{\mathbf{k}} u_{n\mathbf{k},\xi} | \times | \partial_{\mathbf{k}} u_{n\mathbf{k},\xi} \rangle. \quad (9)$$

It is important to note that in a two-dimensional system, the Berry curvature dipole transforms as a pseudo-vector as described by the vector D_i ($i = x, y$). In other words, D_i must be invariant under crystal point group operations. For twisted tWSe₂ with or without the displacement field, the system respects a three-fold rotational symmetry C_{3z} inherited from monolayer 2H-structure WSe₂. Due to the time-reversal symmetry, $\Omega_n(\mathbf{k} + \mathbf{K}) = -\Omega_n(-\mathbf{k} - \mathbf{K})$, $\mathbf{v}_n(\mathbf{k} + \mathbf{K}) = -\mathbf{v}_n(-\mathbf{k} - \mathbf{K})$, each valley has an equal contribution, allowing us to consider the K_+ valley for the sake of simplicity. For K_+ valley, C_{3z} symmetry ensures $\Omega_n(\mathbf{k}) = \Omega_n(C_3\mathbf{k}) = \Omega_n(C_3^2\mathbf{k})$ and $\sum_{i=0}^2 \mathbf{v}_n(C_3^i\mathbf{k}) = 0$. Therefore, D_i vanishes if C_{3z} symmetry is preserved. One way to obtain finite D_i is to take into account the strain effects which break C_{3z} . The strain can be induced by the substrate which couples to tWSe₂ or it can be induced externally as shown in the above sections. As we will see in the next section, only a very small strain is needed to induce a strong NLH response in tWSe₂.

Topological phase transition and NLH effect

With the formalism discussed above, we can now explore the NLH effects in tWSe₂. By applying a uniaxial strain with $\epsilon = 0.5\%$ along the direction of the zigzag edge and at twist angle 1.4° , D_x as a function of the vertical displacement field V_z and the occupation number of holes per moire unit cell n_h are depicted in Fig. 3a. The occupation number n_h is obtained by integrating the

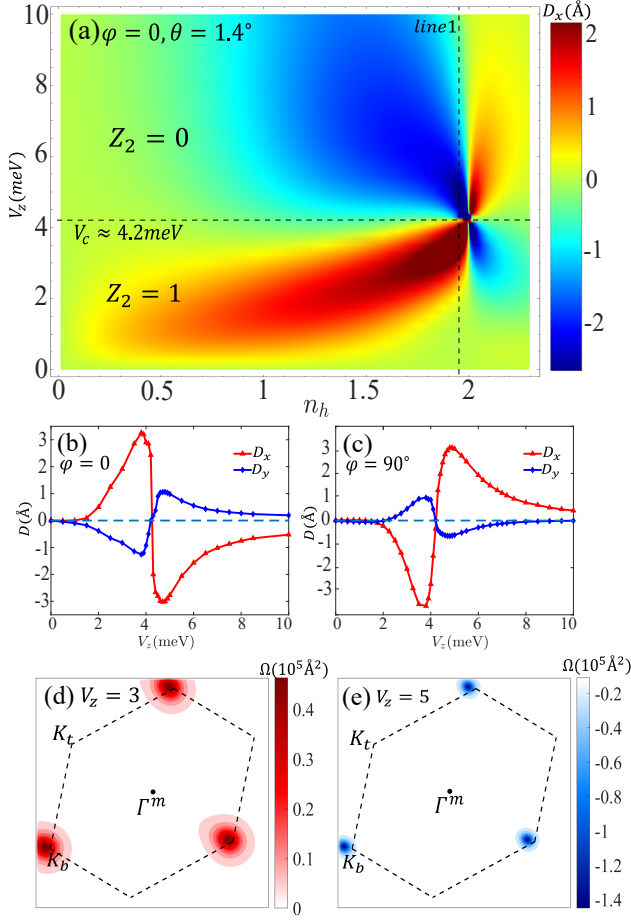


FIG. 3: (a) The V_z and n_h dependence of D_x with strain $\epsilon = 0.5\%$ along the zigzag edge direction. The critical V_z at which the phase transition occurs is denoted by the horizontal dashed line. D_x is strongly enhanced near the phase transition point and $n_h \approx 2$ when the Fermi energy is near the bottom of the top valence band. (b) D_x, D_y as a function of V_z with fixed n_h . The values of n_h ($= 1.95$) are denoted by the vertical line 1 in (a). For (b), an uniaxial strain is applied along the zigzag edge direction. (c) Same parameters as (b) but the uniaxial strain is applied along the armchair edge direction. (d) and (e) The Berry curvatures of top valence band of strained tWSe₂ in the deformed Brillouin zone before and after the topological phase transition respectively. In (d), $V_z = 0$, in (e), $V_z = 5$ meV. The strain is applied along the zigzag edge direction. The temperature is set to $1.5K$.

density of states from the top of the valence to the Fermi energy including two valleys. It is clear from Fig. 3a that the Berry curvature dipole is generally large, in the order of 1Å .

Importantly, the Berry curvature dipole is strongly enhanced near the bottom of the top valence band when n_h is close to 2 (this happens when the Fermi energy is near the bottom of the top valence band) and V_z close to 4.2 meV. Specifically, the bands originating from the K_+ (or K_-) valley have nontrivial topological invariant $Z_2 = 1$.

By applying a displacement field which introduces a potential difference between the top and the bottom layers, the top valence band and the nearby valence band can touch near the K points and exchange Berry curvatures, resulting in a change of Z_2 invariant from 1 to 0[15]. The V_z dependence of the Berry curvature dipole across the phase transition with fixed n_h is shown in Fig. 3b. It is clear that Berry curvature dipole is strongly enhanced near the critical $V_z \approx 4.2$ meV when n_h is close to 2. This value is several times larger than the optimal Berry curvature dipole measured experimentally in other systems which is about 1Å [22, 23]. Moreover, the Berry curvature dipole changes sign across the phase transition point. This is caused by the exchange of Berry curvatures near the K points before and after the topological phase transition as shown in Fig. 3d and Fig. 3e.

Furthermore, the V_z dependence of the Berry curvature dipole with fixed n_h is shown in Fig. 3c when strain is applied along the armchair edge direction. Similar enhancement and sign change in the Berry curvature dipole near the topological phases transition can be observed. In the supplementary materials[31], the V_z and n_h dependence of the Berry curvature dipole with different twist angles and strain are presented and behaviors similar to Fig. 3a are observed. Therefore, the NLH measurements can be used to probe the topological properties of the bands and identify the topological phase transition point.

Discussion

It is important to note that the appearance of NLH effect studied in this work is very general. We expect a finite NLH response as long as the three-fold rotational symmetry is broken intrinsically by the substrate[24] or by an externally applied strain. Recently, correlated insulating phase is observed when the filling factor n_h is close to 1, and this corresponds to half filling in the top valence band which is far from the topological phase transition regime where $n_h \approx 2$. Near the phase transition regime, we expect the system to be metallic and can be described by a Fermi liquid. Nevertheless, the NLH measurements can reveal the topological properties of the bands away from the Fermi energy that shed light on the nature of correlated phases. Furthermore, we point out that strained tWSe₂ and other moire materials are excellent candidate materials for studying NLH effects due to their low symmetry, non-trivial Berry curvature and high tunability of experimental parameters[32, 33]. Following our theoretical predictions, NLH effects in twisted double bilayer WSe₂ have been observed[34].

Acknowledgments

We thank the support of the Croucher Foundation and HKRGC through 16324216, 16307117 and 16309718.

* phlaw@ust.hk

- [1] Bistritzer R., MacDonald, A. H. Moiré bands in twisted double-layer graphene. *Proc. Natl. Acad. Sci. U.S.A.* **108**(30), 12233 (2011).
- [2] Cao, Y. et al. Correlated insulator behaviour at half-filling in magic-angle graphene superlattices. *Nature* **556**, 80 (2018).
- [3] Cao, Y. et al. Unconventional superconductivity in magic-angle graphene superlattices. *Nature* **556**, 43 (2018).
- [4] Lu, X. et al. Superconductors, orbital magnets, and correlated states in magic angle bilayer graphene. *Nature* **574**, 653 (2019).
- [5] Yankowitz, M. et al. Tuning superconductivity in twisted bilayer graphene. *Science* **363**, 10591064 (2019).
- [6] Po, H. C., Zou, L., Vishwanath, A. & Senthil, T. Origin of Mott Insulating Behavior and Superconductivity in Twisted Bilayer Graphene. *Phys. Rev. X* **8**, 031089 (2018).
- [7] Isobe, H., Yuan, N. F. Q. & Fu, L. Unconventional Superconductivity and Density Waves in Twisted Bilayer Graphene. *Phys. Rev. X* **8**, 041041 (2018).
- [8] Wu, F., MacDonald, A. H. & Martin I. Theory of Phonon-Mediated Superconductivity in Twisted Bilayer Graphene. *Phys. Rev. Lett.* **121**, 257001 (2018).
- [9] Liu, C.-C., Zhang, L.-D., Chen, W.-Q. & Yang, F. Chiral Spin Density Wave and $d+id$ Superconductivity in the Magic-Angle-Twisted Bilayer Graphene. *Phys. Rev. Lett.* **121**, 217001 (2018).
- [10] Xie, M. & MacDonald, A. H. Nature of the correlated insulator states in twisted bilayer graphene. *Phys. Rev. Lett.* **124**, 097601 (2020).
- [11] Liu, J., Liu, J. & Dai, X. Pseudo Landau level representation of twisted bilayer graphene: Band topology and implications on the correlated insulating phase. *Phys. Rev. B* **99**, 155415 (2019).
- [12] Koshino, M. et al. Maximally Localized Wannier Orbitals and the Extended Hubbard Model for Twisted Bilayer Graphene. *Phys. Rev. X* **8**, 031087 (2018).
- [13] Zou, L., Po, H. C., Vishwanath, A. & Senthil, T. Band structure of twisted bilayer graphene: Emergent symmetries, commensurate approximants, and Wannier obstructions. *Phys. Rev. B* **98**, 085435 (2018).
- [14] Wu, F., Lovorn, T., Tutuc, E. & MacDonald, A. H. Hubbard Model Physics in Transition Metal Dichalcogenide Moiré Bands *Phys. Rev. Lett.* **121**, 026402 (2018).
- [15] Wu, F., Lovorn, T., Tutuc, E., Martin I. & MacDonald, A. H. Topological Insulators in Twisted Transition Metal Dichalcogenide Homobilayers *Phys. Rev. Lett.* **122**, 086402 (2019).
- [16] Wang, L. et al. Magic continuum in twisted bilayer WSe₂. arXiv: <http://arXiv.org/abs/arXiv:1910.12147>(2019).
- [17] Bi, Z. & Fu, L. Excitonic density wave and spin-valley superfluid in bilayer transition metal dichalcogenide. arXiv: <http://arXiv.org/abs/arXiv:1911.04493>
- [18] Sharpe, A. L. et al. Emergent ferromagnetism near three-quarters filling in twisted bilayer graphene. *Science* **365**, 605-608 (2019).
- [19] Serlin, M. et al. Intrinsic quantized anomalous Hall effect in a moiré heterostructure. *Science* **367**, 6480, 900-903 (2020).
- [20] He, W.-Y., Gordon, D. G. & Law, K. T. Giant Orbital Magneto-electric effect and Current-driven Magnetization Switching in Twisted Bilayer Graphene. *Nat. Commun* **11**, 1650 (2020).
- [21] Sodemann, I. & Fu, L. Quantum Nonlinear Hall Effect Induced by Berry Curvature Dipole in Time-Reversal Invariant Materials. *Phys. Rev. Lett.* **115**, 216806 (2015).
- [22] Ma, Q. et al. Observation of the nonlinear Hall effect under time reversal symmetric conditions. *Nature* **565**, 337342 (2019).
- [23] Kang, K. et al. Nonlinear anomalous Hall effect in few-layer WTe₂. *Nat. Mater.* **18**, 324328(2019).
- [24] Zhang, Z. et al. Flat bands in small angle twisted bilayer WSe₂. arXiv: <http://arXiv.org/abs/arXiv:1910.13068>(2019).
- [25] Facio, J. I. et al. Strongly enhanced Berry dipole at topological phase transitions in BiTeI. *Phys. Rev. Lett.* **121**, 246403 (2018).
- [26] Bi, Z., Yuan, N. F. Q. & Fu, L. Designing Flat Band by Strain. *Phys. Rev. B* **100**, 035448 (2019).
- [27] Kang, J. et al. Band offsets and heterostructures of two-dimensional semiconductors. *Applied Physics Letters* **102**(1), 012111 (2013)
- [28] Fang, S., Carr, S., Casalilla, M. A. & Kaxiras, E. Electronic structure theory of strained two-dimensional materials with hexagonal symmetry. *Phys. Rev. B* **98**, 075106 (2018).
- [29] Zhou, B. T., Zhang, C.-P., & Law, K. T. Highly tunable nonlinear Hall effects induced by spin-orbit couplings in strained polar transition-metal dichalcogenides. *Phys. Rev. Applied*, **13**, 024053(2020).
- [30] Du, Z. Z., et al. Band signatures for strong nonlinear Hall effect in bilayer WTe₂. *Phys. Rev. Lett* **121**, 266601 (2018).
- [31] Supplementary materials.
- [32] Chen, G. et al. Tunable Correlated Chern Insulator and Ferromagnetism in Trilayer Graphene/Boron Nitride Moiré Superlattice. arXiv: <http://arXiv.org/abs/arXiv:1905.06535> (2019).
- [33] Zhang, Y.-H. et al. Nearly flat Chern bands in moiré superlattices. *Phys. Rev. B* **99**, 075127(2019).
- [34] In preparation.